Inorganic Chemistry

pubs.acs.org/IC Article

Sc-HOPO: A Potential Construct for Use in Radioscandium-Based Radiopharmaceuticals

Michael D. Phipps,[†] Shelbie Cingoranelli,[†] N. V. S. Dinesh K. Bhupathiraju, Ali Younes, Minhua Cao, Vanessa A. Sanders, Michelle C. Neary, Matthew H. Devany, Cathy S. Cutler, Gustavo E. Lopez, Shefali Saini, Candace C. Parker, Solana R. Fernandez, Jason S. Lewis, Suzanne E. Lapi, Lynn C. Francesconi, and Melissa A. Deri*



Cite This: https://doi.org/10.1021/acs.inorgchem.2c03931



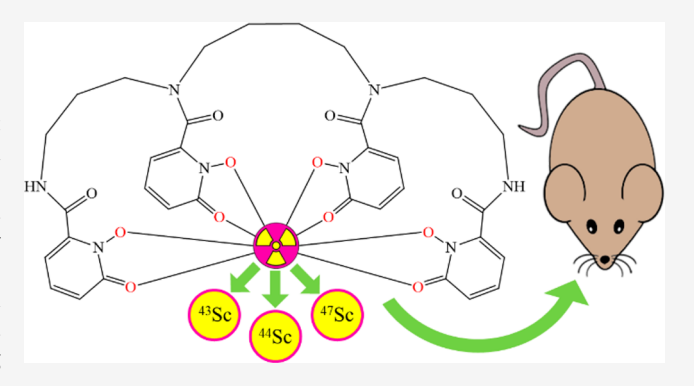
ACCESS

Metrics & More

Article Recommendations

Supporting Information

ABSTRACT: Three isotopes of scandium—⁴³Sc, ⁴⁴Sc, and ⁴⁷Sc—have attracted increasing attention as potential candidates for use in imaging and therapy, respectively, as well as for possible theranostic use as an elementally matched pair. Here, we present the octadentate chelator 3,4,3-(LI-1,2-HOPO) (or HOPO), an effective chelator for hard cations, as a potential ligand for use in radioscandium constructs with simple radiolabeling under mild conditions. HOPO forms a 1:1 Sc-HOPO complex that was fully characterized, both experimentally and theoretically. [⁴⁷Sc]Sc-HOPO exhibited good stability in chemical and biological challenges over 7 days. In healthy mice, [^{43,47}Sc]Sc-HOPO cleared the body rapidly with no signs of demetalation. HOPO is a strong candidate for use in radioscandium-based radiopharmaceuticals.



INTRODUCTION

The strong appeal of personalized medicine has fueled expansion of the library of diagnostic and therapeutic agents that are tailored to optimize individual patient care. This goal has further driven research on the use of radiometals in medicine. Radiometals have a broad spectrum of both chemical and nuclear properties that provide many avenues for the development of new radiopharmaceuticals with different clinical utilities. To date, research into radiometal-based radiopharmaceuticals has yielded Food and Drug Administration (FDA)-approved agents for both imaging and therapy with several radiometals, including ^{99m}Tc, ⁶⁸Ga, ¹¹¹In, ¹⁷⁷Lu, ⁹⁰Y, and more. ¹ Numerous other agents incorporating radiometals are either in clinical trials or under investigation.

The chemical and nuclear properties of a specific radiometal determine its suitability for incorporation into a radio-pharmaceutical agent. For example, the type of radioactive decay that the radiometal undergoes and its half-life determine its potential medical application. The chemistry of the radiometal governs its stable inclusion in a chelator in the drug, and the biological effects should it be released from the chelator. One radiometal recently attracting attention is scandium because it has several accessible isotopes with medical utility, including 43 Sc, 44 Sc, and 47 Sc. 43 Sc ($t_{1/2} = 3.89$ h, $\beta^+_{\rm max} = 1.20$ MeV, and BR $_{\beta+} = 70.9\%$) and 44 Sc ($t_{1/2} = 3.97$ h, $\beta^+_{\rm max} = 1.47$ MeV, and BR $_{\beta+} = 94.3\%$) have emission properties that make them suitable for use in positron emission

tomography (PET) imaging. 247 Sc ($t_{1/2} = 3.35$ d, $\beta^-_{max} = 0.6$ MeV, and BR $_{\beta^-} = 100\%$) has emission properties suitable for targeted radiotherapy and radioimmunotherapy (RIT), also possesses a single γ emission (159 keV, BR $_{\gamma} = 68\%$) that is similar to that of $^{99\text{m}}$ Tc (140 keV, BR $_{\gamma} = 89\%$), and has the potential for application in single photon emission computed tomography imaging. In combination, these different radioisotopes of scandium can be used to create chemically identical radiopharmaceuticals that can be used for both therapeutic and diagnostic applications, i.e., theranostic agents. Additionally, because 47 Sc alone has both therapeutic β^- and imageable γ emissions, it can be used toward the development of a single true theranostic agent. 2

The half-lives of ⁴³Sc and ⁴⁴Sc render them appropriate for use with small molecules and peptides, whose *in vivo* kinetics are faster than monoclonal antibodies (mAbs), or with pretargeted strategies using mAbs. The longer half-life of ⁴⁷Sc is appropriate for use with mAbs in RIT because radioimmunoconjugates may need to circulate for a few days

Special Issue: Inorganic Chemistry of Radiopharmaceuticals

Received: November 7, 2022



Figure 1. Structural scheme for the HOPO ligand and the Sc-HOPO complex, with the coordinating O atoms shown in red.

before accumulating at their target. The longer half-life does not preclude it from use in pretargeting, and so both ^{43/47}Sc and ^{44/47}Sc could be used in a pretargeted theranostic system, with the nuclides being exchanged in either a diagnostic or therapeutic context, respectively.

Radiometals require a chelator for stabilization and incorporation into a pharmacophore. The role of the chelator is to bind the radiometal and ensure a stable complex, at least until the biological target is reached. The 1,4,7,10-tetraazacy-clododecane-1,4,7,10-tetraacetic acid (DOTA) ligand is considered a relatively universal chelator and has been used for a variety of radiometals, including ¹⁷⁷Lu, ⁶⁸Ga, and ⁹⁰Y clinically. DOTA has been used to create and evaluate radioscandium-based constructs in both preclinical and early clinical work. ^{3–11} Recently, the production and accessibility of a wider library of radiometals prompted demand for new chelators designed with their particular chemistry in mind. ^{12,13}

In some cases, the conditions needed for the chemical synthesis of radiometal complexes are incompatible with the conjugated targeting molecule. For example, syntheses with DOTA conjugates generally employ reaction temperatures of 60–95 °C that are incompatible with mAbs.^{7,8,14,15} Overcoming this obstacle involves drawbacks such as longer synthesis time that is detrimental to nuclides with short half-lives, prolonged exposure to workers, and potential degradation of the functional group that conjugates to the protein.

Sc is the first transition metal and is a part of the rare-earth elements (REEs). It forms a trivalent ion with coordination chemistry similar to other REE ions such as Y3+, with a preference for octadentate coordination complexes. Sc3+ is a small, hard ion with a preference for hard donor groups such as O or N. So far, radioscandium complexes have been reported with both cyclic and acyclic polyaminopolycarboxylate chelators. $^{4,16-21}$ A significant portion of radioscandium in vivo work has been performed with small-molecule conjugates using DOTA as the chelator. 8,15 These studies have used small molecules as targeting vectors, including DOTA-octreotate (DOTATATE), prostate-specific membrane antigen (PSMA), and folate, that can be labeled at high temperatures. At lower labeling temperatures, there is the risk for the formation of "out-of-cage" complexes, where a metal cation is bound by the O atoms on the pendant arms but not within the N_4 ring of the ligand, thus compromising the stability of the construct and increasing the likelihood of the metal being released.⁴ Other chelators such as CHX-A"-DTPA, AAZTA, and H₃mpatcn have been used for *in vivo* studies as well. ¹⁹⁻²¹ Both CHX-A"-DTPA and H₃mpatcn have exhibited radiolabeling at room temperature (RT). Investigation of a variety of "old" and "new" ligands will allow the development of a better optimized chelate system for efficient labeling under mild conditions and for increased complex stability.

3,4,3-(LI-1,2-HOPO) (or HOPO, Figure 1) is an acyclic chelator that has demonstrated a strong affinity for hard metal

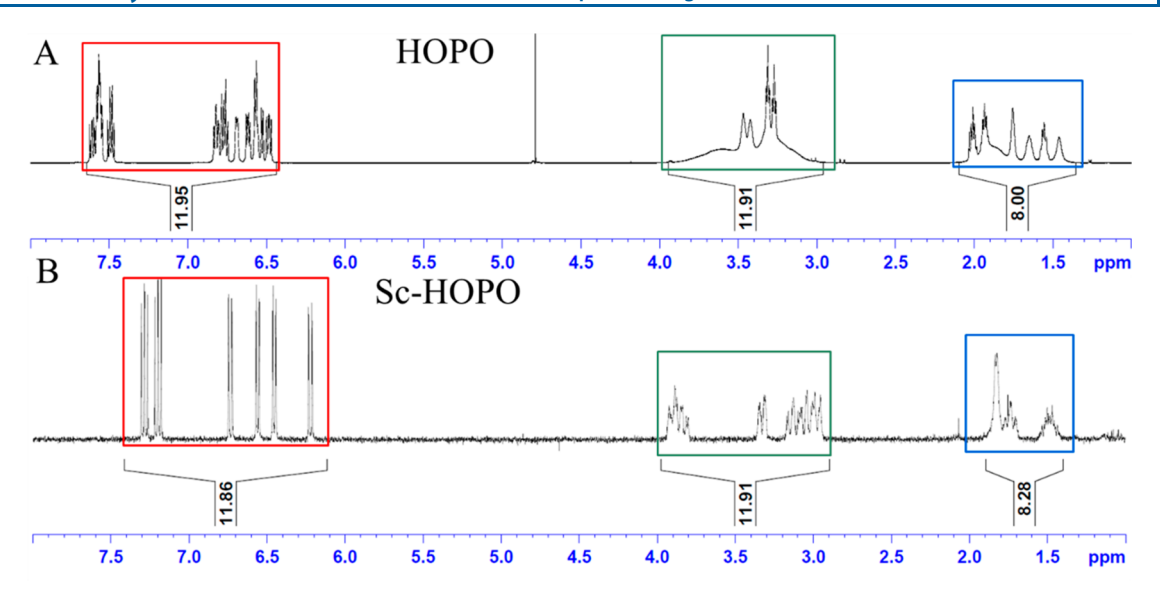


Figure 2. ¹H NMR spectra of HOPO and K[Sc(HOPO)] in D₂O. Corresponding integral regions are highlighted by color.

3+ and 4+ ions. $^{22-26}$ It has been previously demonstrated as a superior chelator for 89 Zr with less *in vivo* demetalation than 89 Zr-DFO, the clinically used chelator. HOPO is an 8-coordinate ligand with hard O-donating groups that are suitable for Sc^{3+} ion, which typically produces 8-coordinate complexes, with 7- and 6-coordinate species also known. $^{27-29}$ HOPO has also been demonstrated to form complexes with metals at a lower pH than DOTA, and the acyclic arrangement should result in faster binding kinetics compared to a macrocycle. A bifunctional p-SCN-Bn-HOPO that can be conjugated to biomolecules has previously been developed, evaluated, and synthetically optimized. 23,30

In this study, we investigate the radiolabeling, characterization, stability, and *in vivo* behavior of $[^{43/44/47}Sc]Sc$ -HOPO as well as the synthesis and characterization of the macroscopic Sc-HOPO complex. These experiments demonstrate the potential for HOPO as a chelator for the development of radioscandium-based agents.

■ RESULTS AND DISCUSSION

The design and selection of chelators for radioscandium should focus on best meeting the specific chemical properties of the Sc³⁺ ion. Our criteria for an ideal chelator for Sc are as follows. An octadentate ligand offers the potential to fully saturate the coordination sphere of Sc3+. Hard O-donor groups are desirable to complement the hard Sc³⁺ cation. The chelator must also have a properly sized cavity for the 1.01 Å effective ionic radius for 8-coordinate Sc^{III}. 31 Acyclic chelators are preferred because their flexibility should facilitate faster kinetics for more efficient radiolabeling conditions. By combining these properties within one molecule, the HOPO ligand is a strong candidate as a potential chelator for Sc³⁺. Herein, we have paired our macroscopic characterization, radiochemistry, and stability studies with density functional theory (DFT) studies to confirm the performance and stability of the Sc-HOPO complex.

Synthesis. The HOPO ligand was synthesized as previously reported with minor augmentations. ^{24,32,33} The final product was reverse-phase high-performance liquid chromatography (HPLC)-purified to remove trace impurities

that could potentially interfere with radiolabeling. The synthesis is given in Scheme S1 and Figure S1.

The symmetry and flexibility of HOPO result in an ¹H NMR spectrum with many overlapping multiplets and broad peaks due to coexisting conformers in solution. Mass spectrometry and HPLC analysis, Figures S2A and S3A, respectively, corroborate HOPO as a single compound. HOPO picks up Fe^{III} very easily, and therefore it is common to observe Fe-HOPO in liquid chromatography—mass spectrometry (LC—MS).³⁴

Nonradioactive, macroscopic Sc-HOPO was synthesized and characterized for comparison with the tracer Sc-HOPO. ScCl₃ was added to an aqueous solution of HOPO in a 1:1.1 ratio of HOPO-to-Sc in water at RT. Upon the addition of ScCl₃ to the solution of HOPO, a white precipitate formed almost immediately, and the solution became milky. The Sc-HOPO complex has relatively low solubility, especially under acidic conditions. The precipitate redissolved as the pH was raised by the addition of K2CO3. If the pH rises above 7 and becomes basic, a new precipitate will form. This is unreacted Sc precipitating as Sc(OH)3, which is insoluble under mildly basic conditions. The reaction mixture was filtered through a 0.2 μ m syringe filter to remove Sc(OH)₃. The resulting complex of Sc-HOPO carries a charge of 1-, and so K₂CO₃ was also used to provide a K⁺ counterion to the complex. The filtered solution was then lyophilized to dryness. K[Sc-(HOPO)] was purified by reverse-phase HPLC and lyophilized to a powder.

Characterization. High-resolution mass spectrometry (HRMS) of the product dissolved in water identifies the Sc-HOPO complex with the expected mass signals (793.2008 Da for [M + 2H]⁺ and 815.1821 Da for [M + H + Na]⁺; Figure S2B). Analytical HPLC of the product dissolved in water shows a peak at a retention time of 5.35 min that tails slightly, with another small peak at 6.29 min (Figure S3B). The HPLC and LC–MS chromatograms both exhibited a long tail following the primary peak. Mass analysis of the primary peak and tail region indicates that only the mass of Sc-HOPO is present in all regions of the tail and primary peak. This indicates the presence of an alternative species of Sc-HOPO that interacts slightly differently with the column. An

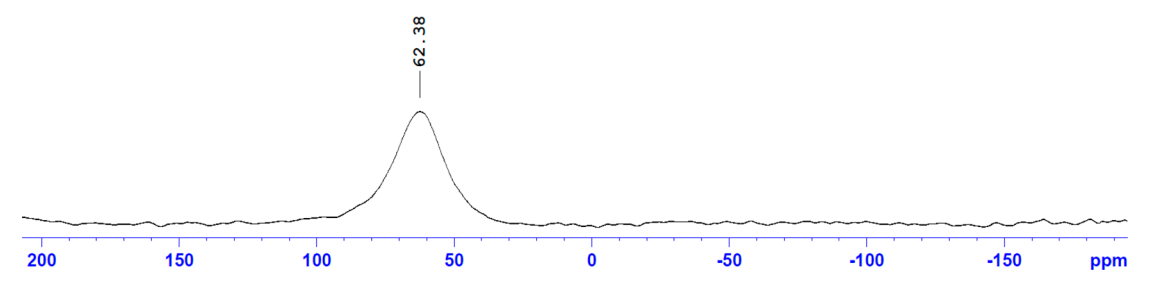


Figure 3. 45 Sc NMR spectrum of K[Sc(HOPO)] in D₂O. The broad peak (fwhm = 12414 Hz) is consistent with the 45 Sc NMR spectra of other Sc chelates. 0.1 M ScCl₃ in 0.01 M HCl was used as the reference standard for the NMR method.

alternative Sc-HOPO species was indicated in ¹H NMR studies as a function of the pH, and the formulation of the potential species was examined by DFT calculations, *vide infra*.

Figure 2 shows the ¹H NMR of Sc-HOPO and the HOPO ligand in D₂O at pH 7. The ¹H NMR spectrum of the Sc-HOPO complex shows overlapping multiplets in the aliphatic region similar to the ¹H NMR spectrum of HOPO, however with less broadness. The peaks in the aromatic region, most associated with the binding of hydroxypyridinonates to Sc³⁺, experienced the most significant change, with clean, discrete peaks indicative of binding to the metal center, locking the electronic environments of those protons. This is in contrast to the ¹H NMR spectra of Zr-HOPO described by Deri et al., in which the aromatic region showed a complex set of overlapping multiplets.²⁴

⁴⁵Sc is a quadrupolar nucleus that is easily probed even at low concentrations by ⁴⁵Sc NMR due to its sensitivity. Additionally, it is monoisotopic, so there are no other isotopes of Sc macroscopically to dilute an NMR signal. ⁴⁵Sc NMR (Figure 3) shows a single broad peak at 62.38 ppm with a large full-width at half-maximum (fwhm) of 12414 Hz that is consistent with other Sc chelate compounds, such as Sc-DOTA, Sc-DTPA, Sc-EDTA, Sc-AAZTA, and Sc-mpatcn. 18,20,35,36 The analysis of liquid samples of Sc chelates by ⁴⁵Sc NMR tends to give broad peaks that are shifted down range (>50 ppm) from the reference. The broadness may result from the asymmetry of the ligand field in Sc-HOPO compared to the highly symmetric $Sc(H_2O)_6^{3+}$ ion in the reference standard. Because ⁴⁵Sc is a quadrupolar nucleus, peak broadening is expected in the case of asymmetric ligand fields. An asymmetric ligand can arise from a nonfluxional environment of the chelate, which is expected from the 8-coordinate structure provided by the chelation of Sc^{III} by HOPO. 18,37,38 This has been observed in a comparison of the Sc-DTPA and Sc-DOTA systems. 18,35,37,38 The chemical shift is consistent with full encapsulation of the Sc3+ nucleus by the hydroxypyridinonate groups, resulting in the Sc3+ nucleus being highly shielded. The formation of "out-of-cage" complexes tends to give shifts in a lower range of 20-30 ppm. 4,18,39 A lower chemical shift in this range is due in part to the poor shielding of the Sc3+ nucleus from solvent molecules in comparison to a fully chelated metal center without coordinating solvent molecules.^{4,20} Additionally, it is expected to see a narrower peak width in the case of out-of-cage complexes than to see a more fluxional environment. 18,35 This downfield broad peak observed for the Sc-HOPO sample supports its identification as an in-cage, asymmetric single structure. Hence, the ⁴⁵Sc NMR evidence indicates complete chelation of the Sc³⁺ nucleus by the HOPO chelator.

A K[Sc(HOPO)] crystal structure was obtained previously by Carter et al. and contained N,N-dimethylformamide (DMF) in the lattice. ⁴⁰ In this work, crystals of K[Sc(HOPO)] in the form of $\{K(OH_2)_2[Sc(HOPO)]\}_2$ were obtained by the slow evaporation of a solution of K[Sc(HOPO)] with K₂CO₃ and KCl in water over 8 weeks without any DMF present. A single crystal from this sample was taken and analyzed by X-ray crystallography. The details of the crystal, intensity collection, and refinement data are shown in Table S1. Relevant bond lengths and angles are shown in Table S2. The crystal structure is shown in Figure 4. The resulting structure is a racemic pair

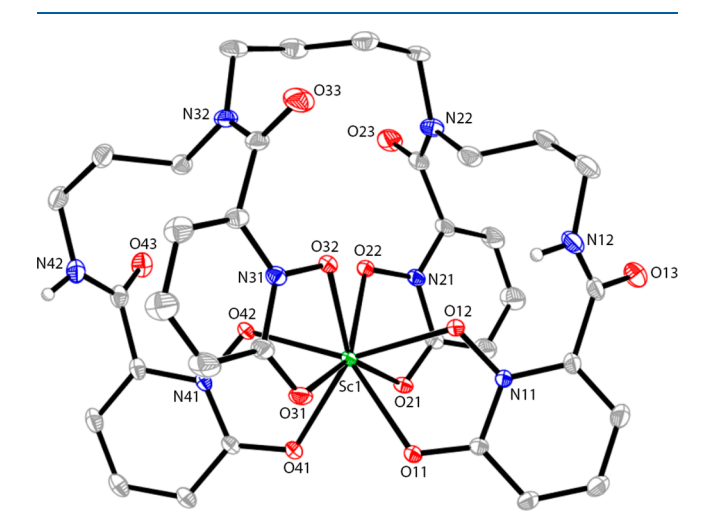


Figure 4. Molecular diagram of the Sc-HOPO anion. H atoms bound to C atoms as well as disordered C atoms in the HOPO backbone are omitted for clarity. Atomic displacement parameters are displayed at the 30% probability level.

of enantiomers in a monoclinic space group $(P2_1/c)$ with only H₂O in the lattice, in contrast to the Carter et al. structure, which contained a racemic pair of Sc-HOPO units in a triclinic space group $(\overline{P1})$ with both H_2O and DMF. There are, however, some similarities in the complexes themselves. Both structures display a racemic pair of 8-coordinate Sc-HOPO complexes with a distorted square-antiprismatic geometry around the metal center. In this structure, two enantiomeric Sc-HOPO units are bridged by two K⁺ units. The complexes exhibit $\Delta(\delta)$ - and $\Lambda(\lambda)$ - handedness according to the orientation of the butylenediamine portion of the ligand backbone relative to the metal center. Such isomerism has been observed in other metal complexes with HOPO, such as in Zr-HOPO.²³ As noted by Carter et al., it has yet to be determined whether the enantiomers of Sc-HOPO are separable. 40 There is a small amount of disorder in the flexible

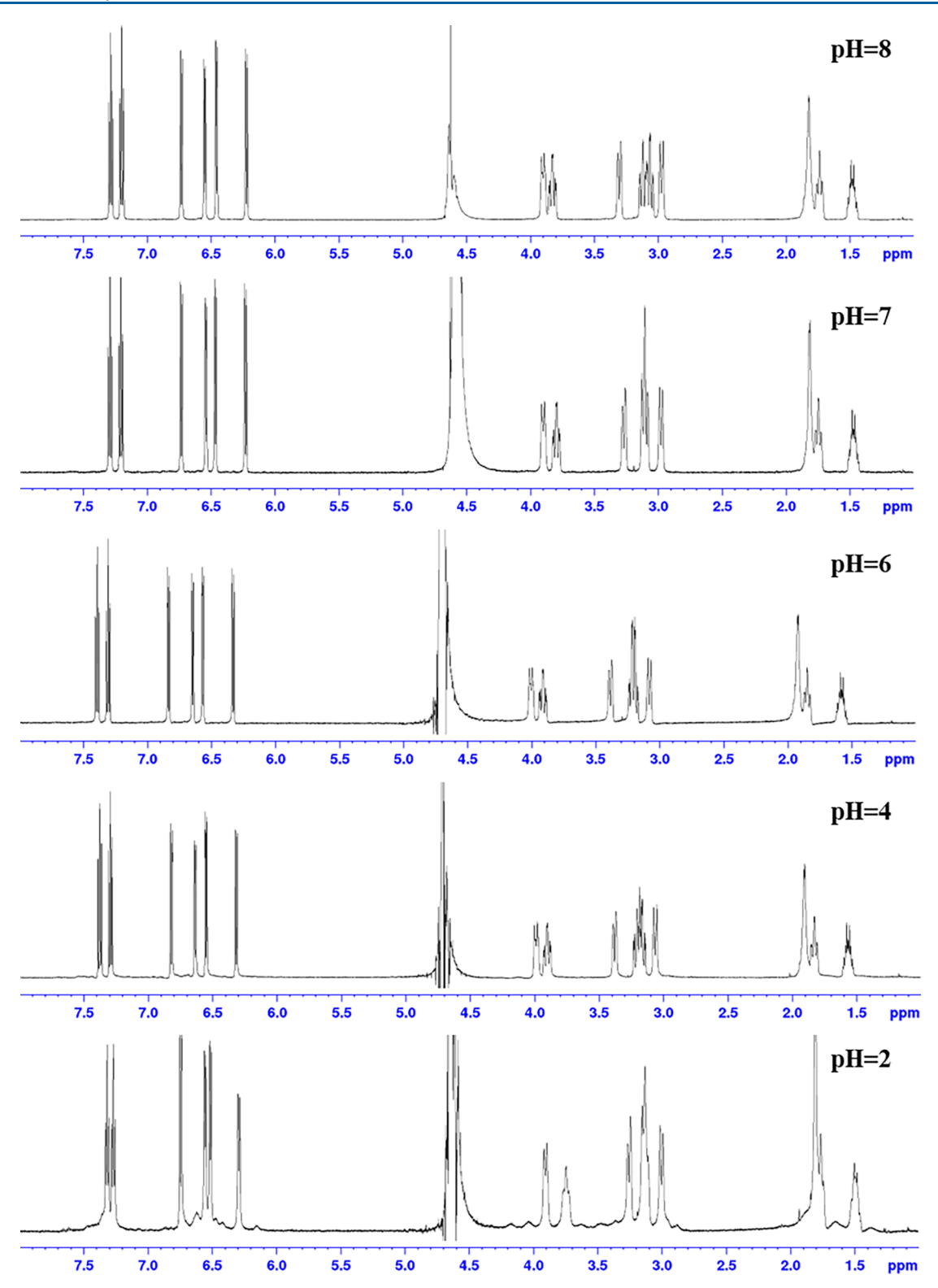


Figure 5. 1 H NMR spectra of K[Sc(HOPO)] taken at different pH values in D₂O. The pH was measured by a pH probe, which introduced H₂O to the sample. Although peak suppression for H₂O was used in the NMR method, the quantity of water was too great for it to be effective. The pH was adjusted with K₂CO₃ and DCl. The resultant increase of the KCl concentration results in minor chemical shift changes for both the analyte and solvent peak.

alkyl backbone of the ligand, as well as disorder from the solvent and K bridges. The average Sc–O bond length was 2.221 Å, which is slightly longer than the 2.213 Å average bond length reported by Carter et al.⁴⁰ The small difference in the reported average bond length may be related to the different

packing conditions of the crystals. There was no clear pattern regarding the differences in individual Sc-O bond lengths, which ranged from 2.1790(17) to 2.2658(17) Å. The inner and outer hydroxypyridinonate groups on either side of the metal center each bind to Sc opposite from its corresponding

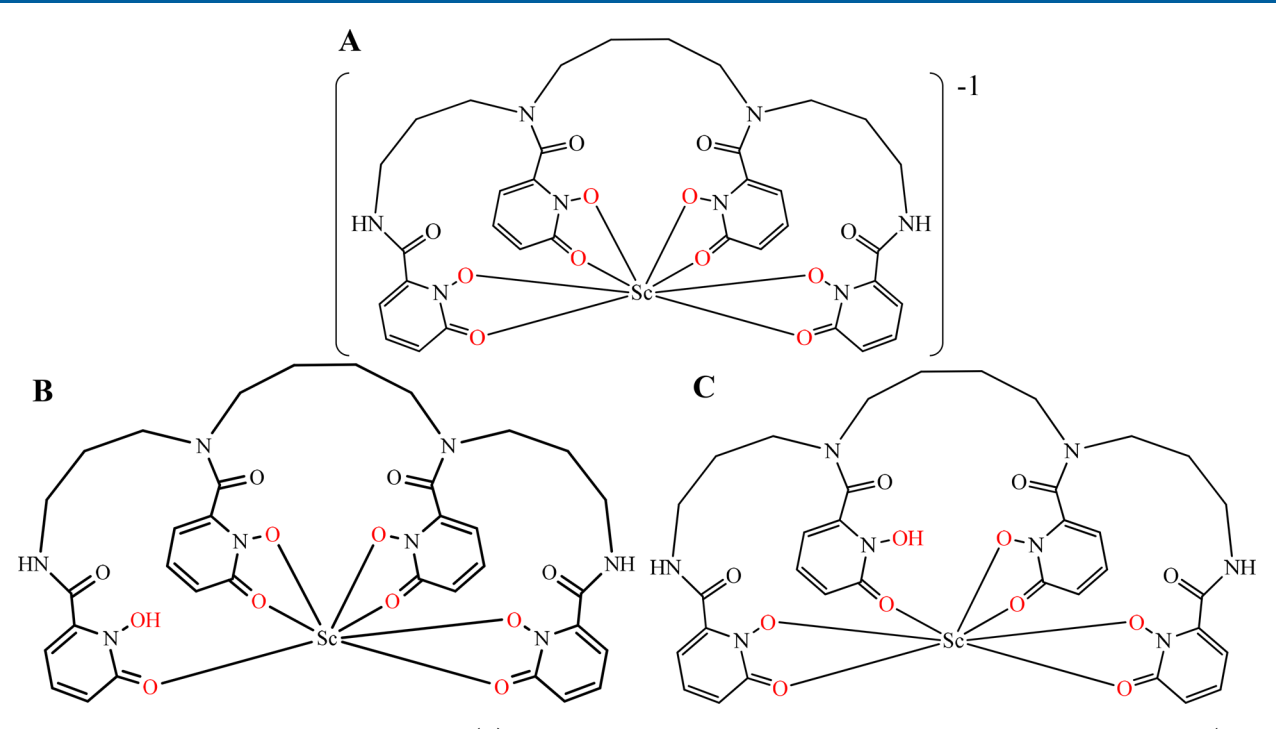


Figure 6. 8-coordinate structural scheme of Sc-HOPO (A) and alternative 7-coordinate schemes for Sc-HOPOH in low pH conditions (B and C).

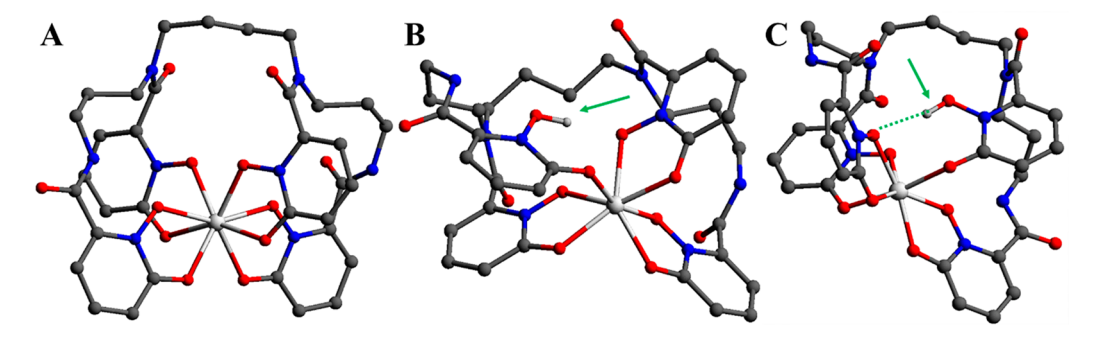


Figure 7. Optimized equilibrium structures for the (A) 8-coordinate complex, (B) 7-coordinate structure with outer group protonation, and (C) 7-coordinate complex with inner group protonation. All H atoms are omitted except for the protonated OH groups in complexes B and C, which are designated by green arrows. A dashed line indicates hydrogen bonding.

hydroxypyridinonate group on the other half of the ligand; the inner hydroxypyridinonate groups are opposite one another, and the outer hydroxypyridinonate groups are opposite one another. An isomer where an inner and outer hydroxypyridinonate group are opposite one another around the Sc center has not been observed. This product may not form due to steric hindrance from the bending of the backbone that would occur in that case. Corroborating the overall connectivity and structural features of the Sc-HOPO anion, this structure was the basis for successful DFT calculations, *vide infra*.

Fourier transform infrared (FT-IR) and UV—vis spectra of HOPO and Sc-HOPO were measured and compared. These can be found in Figures S5 and S6, respectively. The FT-IR samples were solid powders pressed under a mechanical arm for attenuated total reflectance (ATR). In the FT-IR spectra, peak changes from HOPO to Sc-HOPO (from 1633 to 1610 cm⁻¹ and from 1529 to 1515 cm⁻¹) are characteristic of redshifting in C—O vibrations that occur when hydroxypyridinonate binds a metal.²⁴ The UV—vis experiments were done on liquid samples at pH 7. This also shows redshifting in the absorbance maxima between HOPO and Sc-HOPO. HOPO

has maxima at 222 and 308 nm, while Sc-HOPO has maxima at 226 and 315 nm.

¹H NMR as a Function of the pH Suggests Minor **Species at Low pH.** As the pH is decreased from 8 to 2, broad and poorly defined peaks grow in the ¹H NMR spectra (Figure 5), indicating a minor species growing in as the acid content increases. This minor species exists in equilibrium with the dominant Sc-HOPO species under acidic conditions and thus could not be isolated and analyzed separately. The low solubility of Sc-HOPO under acidic conditions also contributed to the poor resolution of the peaks in the minor species. Stability constant measurements and the speciation diagram reported by Carter et al. suggest that this minor species is very likely Sc-HOPO with the addition of a proton. In that study, the protonated Sc-HOPOH species forms in the pH region of -2 to 4.40 Our NMR data are consistent with Sc-HOPOH existing as a minor species at pH 2. Below pH 2, we encountered solubility issues in our sample that made us unable to collect suitable ¹H NMR spectra at lower pH values because there would be too little sample in solution. It is important to note that this process is reversible: increasing the pH to neutrality returns the ¹H NMR spectrum to the original

spectrum at pH 8. This reversible speciation change, as a function of the pH, underlies the stability of the Sc-HOPO species. The use of DCl and $\rm K_2CO_3$ to adjust the pH of the $^1\rm H$ NMR samples resulted in the presence of KCl in solution. This varying concentration of KCl in the samples resulted in minor chemical shift changes of the peaks; the other features of the peaks remained the same. The effects of the salt concentration on the chemical shift of the signals were verified by $^1\rm H$ NMR following the addition of KCl to Sc-HOPO samples without altering the pH. This speciation is also reflected in the HPLC data where an acidic mobile phase is employed (0.1% TFA). In the HPLC data, *vide supra*, the major peak tails into a second minor Sc-HOPO species.

The proposed structures for the conformations of this protonated species are shown in Figure 6. In one case, the hydroxyl group on an "outer" hydroxypyridinonate group is protonated and released from the Sc center to form a 7-coordinate complex (Figure 6B). In the second case, the hydroxyl group on an "inner" hydroxypyridinonate group is protonated and released from the Sc ion (Figure 6C). Both scenarios would result in flexible constructs that would manifest as broad peaks in the NMR spectrum. DFT calculations were employed to interrogate these species further.

OFT Calculations. Figure 7 shows the lowest-energy equilibrium structures of the 8- and 7-coordinate complexes. For these calculations, only one isomer from the racemic mixture was considered for the optimized structures and reaction energetics. This was chosen in part for simplicity because the isomers should be nearly identical regarding their bond distances and energetics within a protonation reaction. Like the crystal structure, the optimized 8-coordinate complex (Figure 7A) has a distorted square-antiprismatic structure around the Sc center; the Sc is coordinated to the eight O atoms from the four hydroxypyridinonate units of HOPO. Table 1 shows that the average Sc—O bond for the 8-

Table 1. Average Bond Lengths and Angles for Sc-HOPO and Sc-HOPOH a

system	$\langle R_{\rm Sc-O} \rangle$ (Å)	$R_{\mathrm{O-H}}$ (Å)	$A_{O-H\cdots H}$ (deg)
8-coordinate complex A	2.25(2)		
7-coordinate complex B	2.19(2)	3.02	20
7-coordinate complex C	2.19(2)	1.96	15

 $\ensuremath{^{\prime\prime}}\xspace(R_{Sc-O})$ is average Sc and O bond length, $R_{\rm OH}$ is the distance between the H atom in the protonated hydroxypyridinonate and the O atom in the adjacent unprotonated hydroxypyridinonate, $A_{\rm O-H\cdots H}$ is the angle between the OH group in the protonated hydroxypyridinonate and the O atom in the adjacent unprotonated hydroxypyridinonate.

coordinate complex (A) is 2.25 Å, which is similar to the value obtained for the crystal structure (2.21 Å). Parts B and C of Figure 7 show the optimized structures for the 7-coordinate B and C complexes, where a proton is located on the outer and inner hydroxypyridinonate moieties, respectively. From Table

1, we notice that, in the 7-coordinate complex C, the distance between the H atom in the protonated hydroxypyridinonate and the O atom in the adjacent hydroxypyridinonate is 1.98 Å, and the angle between the OH group in the protonated hydroxypyridinonate and the O atom in the adjacent unprotonated hydroxypyridinonate is 15°, signaling the formation of a hydrogen bond. In the case of the 7-coordinate B complex, the formation of a hydrogen bond is not observed.

Table 2 shows the changes in electronic energy and thermodynamic properties for the formation of the complexes (see Rxn 1 and Rxn 2 and Materials and Methods). For the 8coordinate complex A, it can be observed that ΔE_e and ΔG_s in solution are <0, suggesting that this complex is stable electronically and thermodynamically. Moreover, $\Delta H_s < 0$ and $\Delta S_s > 0$, indicating that the 8-coordinate complex is stabilized by both energetic and entropic contributions. Although smaller in magnitude, the same electronic and thermodynamic stabilization is observed for the 7-coordinate complexes. In this case, the 7-coordinate complexes are thermodynamically stabilized by only the enthalpic contribution. The 7-coordinate C complex is 5.5 kcal/mol more stable than the 7-coordinate B complex. This suggests that the minor species observed in the NMR, HPLC, and stability constant measurements is the 7-coordinate protonated species C. The enhanced stability of complex C over B can be attributed to the formation of a hydrogen bond between the protonated N atom on the hydroxypyridinonate and the O atom on the adjacent inner hydroxypyridinonate.

For the 7-coordinate Sc complexes, additional calculations were performed with an additional H_2O or OH placed in the proximity of Sc to allow for the formation of an 8-coordinate complex. In all cases, H_2O or OH did not coordinate to Sc but rather remained unbound to the complex.

The last column in Table 2 shows the highest occupied molecular orbital (HOMO)—lowest unoccupied molecular orbital (LUMO) energy gap (the energy difference between the LUMO and HOMO), and Figure 8 shows the orbital energy level diagram for each complex. As expected for molecules with highly delocalized π orbitals, the energy gap is relatively large. However, the energy gap of the 7-coordinate C complex is approximately 0.5 eV larger than that of the 7-coordinate B complex. As previously discussed elsewhere, alarger energy gap implies a more stable system. Hence, the 7-coordinate C complex is more stable than the 7-coordinate B complex in terms of the energy gap, in agreement with our electronic structure energy differences and thermodynamic results.

When the frontier orbitals for the complexes are examined, several interesting features can be observed. For the HOMO, (i) the 8-coordinate complex has the electronic cloud equally distributed between the four hydroxypyridinonate moieties, with only an 18% contribution of the Sc, and (ii) the 7-coordinate complexes have the electron cloud distributed between three hydroxypyridinonate groups, with the one not

Table 2. Changes in the Electronic Energy, Gibbs Free Energy, Enthalpy, and Entropy for Formation of Complexes Defined by reactions 1 and 2

system	$\Delta E_{\rm e}({ m kcal/mol})$	$\Delta G_{ m s}({ m kcal/mol})$	$\Delta H_{\rm s}({ m kcal/mol})$	$\Delta S_{\rm s}({ m cal/mol})$	HOMO-LUMO gap (eV)
8-coordinate complex A	-118.1	-88.8	-52.2	120.0	3.8
7-coordinate complex B	-30.3	-25.5	-26.5	-3.3	3.7
7-coordinate complex C	-35.1	-31.0	-32.2	-3.2	4.2

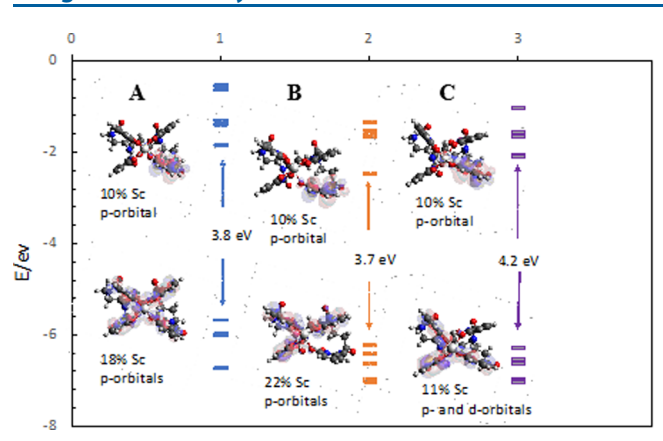


Figure 8. Five LUMO and five HOMO energies for the 8-coordinate A (1 in the x axis), 7-coordinate B (2 in the x axis), and 7-coordinate C (3 in the x axis) complexes. Frontier orbital representations for the LUMO and HOMO for each complex are shown.

having electron density being the protonated hydroxypyridinonate. It can be noticed that the contribution of the metallic orbitals is less in the 7-coordinate complex C than the other two complexes. In the case of the LUMO, all complexes show the same electronic distribution, located in one of the hydroxypyridinonate groups and only a 10% contribution of the p orbital of the Sc.

Radiolabeling. 44Sc was obtained in 2 M HCl from a ⁴⁴Ti/⁴⁴Sc generator system, evaporated to dryness, and reconstituted in a 100 mM ammonium acetate solution at pH 5. Radiolabeling was performed in a pH 5 ammonium acetate buffer with 250 µM ligand, either DOTA or HOPO. The reactions were shaken for 30 min with DOTA heated at 95 °C and HOPO heated at 37 °C. The thin-layer chromatography (TLC) results from the radiolabeling can be found in Figure S8. The plastic-backed silica gel thin-layer chromatography (ITLC-SG) strips were developed using 50 mM ethylenediaminetetraacetic acid (EDTA) at pH 5. Under these conditions, "free" 44Sc should be captured by EDTA and move with the solvent front. The radio-TLC of free 44Sc shows a portion of the activity bound to the origin. This is a result of the formation of oxides or hydroxides of Sc precipitating out of the solution as insoluble particles that stick to the origin on the TLC plate. These particles form under elevated pH conditions and can be difficult to avoid when radioscandium is added from the acidic solution collected from radionuclidic purification to the buffer solution used in radiolabeling. These particles may sometimes be recovered by dissolution in concentrated HCl. However, the activity loss from oxide formation may be irreversible. Both cases have been observed upon radiolabeling with radioscandium. Harshly raising the pH of the solution containing radioscandium causes more particle formation. Particle formation also appears to worsen with the age of the radioscandium solution. The use of a minicentrifuge, $0.2 \mu m$ syringe filter, or C18 sep-pak was effective for removing particles. We consider that the size of the particles at the tracer level made these methods ineffective. The [44Sc]Sc-DOTA and [44Sc]Sc-HOPO complexes migrate with an R_f value of 0.2 that is separated from the 44Sc oxides. Both [44Sc]Sc-DOTA and [44Sc]Sc-HOPO were labeled with >95% radiolabeling yield.

⁴³Sc and ⁴⁷Sc were collected in 0.1 M HCl, evaporated to dryness, and reconstituted in a 0.25 M ammonium acetate solution pH 4. HOPO and DOTA were labeled with radioscandium in a 0.25 M ammonium acetate buffer at pH

4 at 37 °C and are pH 4 at 95 °C, respectively. Yields were >95%, as determined by the ITLC-SG strips in 50 mM EDTA. The free radioscandium moved completely with the solvent front while labeled constructs moved with a $R_{\rm f}$ value of 0.65. Reactions at more acidic pH values as well as at RT were tried to determine the boundaries of viable radiolabeling conditions. Labeling of HOPO was achieved at RT and pH 7 (>95%), while DOTA did not show any radiolabeling. Up to 80% radiochemical yield (RCY) were obtained with HOPO at pH 1 and 37 °C, while DOTA did not label at all.

A coelution of [47Sc]Sc-HOPO with characterized macroscopic Sc-HOPO was performed (Figure 9). An aliquot (~1

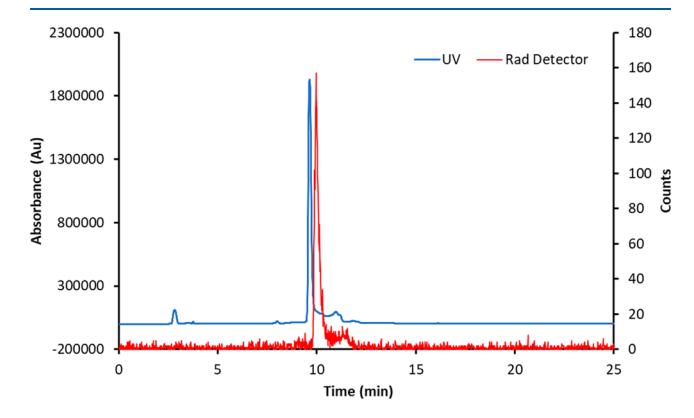


Figure 9. Coelution of [⁴⁷Sc]Sc-HOPO with macroscopic, characterized Sc-HOPO. As discussed above, both macroscopic and tracer levels show tailing caused by Sc-HOPOH.

 μ Ci) of radiolabeled [47 Sc]Sc-HOPO was added to a solution containing 10 mM Sc-HOPO. The elution profiles match well. There is a slight lag time between the profiles from each detector due to the distance between the UV and radiation detectors. This coelution demonstrates that [47 Sc]Sc-HOPO possesses the same structure and chemistry, including the minor protonated species, that was found for the macroscopic Sc-HOPO, thus validating the synthesis of the desired [47 Sc]Sc-HOPO in the radiolabeling reaction.

Stability Studies. To assess the stability of radioscandium complexes over time, [⁴⁷Sc]Sc-DOTA and [⁴⁷Sc]Sc-HOPO were subjected to studies where the complexes were "challenged" with EDTA, pH, and other metal ions.

The [47Sc]Sc-DOTA and [47Sc]Sc-HOPO stability challenges with EDTA both showed high stability, >93% for [47Sc]Sc-HOPO for all constructs and 100% for all [47Sc]Sc-DOTA constructs, as shown in Figure 10, attesting to the high stability of the 47Sc constructs.

The $[^{47}Sc]Sc$ -DOTA complex remained 100% intact at pH 5–8. The $[^{47}Sc]Sc$ -HOPO complex shows similar robustness because most complexes remain 100% intact over the course of 7 days with a slight decrease at pH 6 (93%). These results show that HOPO is a comparable chelator to DOTA in the presence of EDTA.

Additional studies examined the influence of other metal ions on the chelators. Figure 11 represents the results of the metal challenge for DOTA and HOPO complexes.

[47Sc]Sc-DOTA is stable in the presence of Fe, Cu, and Mg for up to 7 days. In the [47Sc]Sc-HOPO metal challenge, HOPO is shown to decomplex in the presence of Fe and Cu within the first day. Both complexes are shown to be unstable in the presence of Zn, with HOPO decomplexing within the

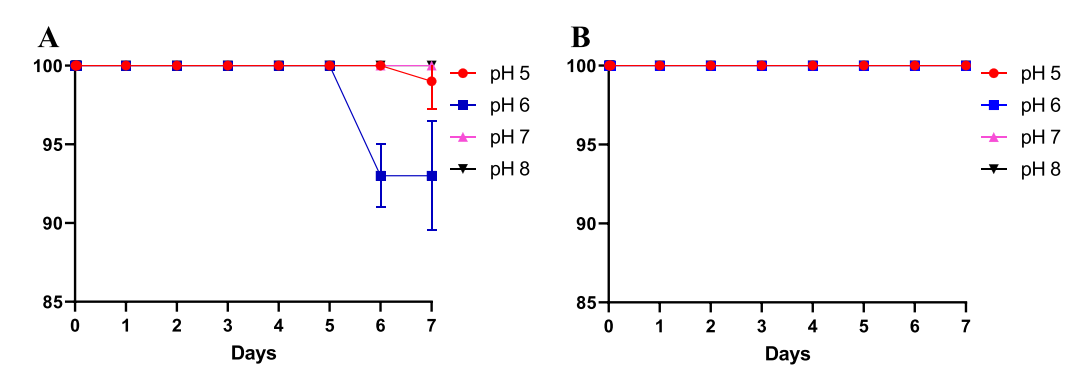


Figure 10. Stability study of [47 Sc]Sc-HOPO over the course of 7 days in the presence of 100 μ M EDTA at varying pH (A). Stability of [47 Sc]Sc-DOTA in the presence of 100 μ M EDTA at varying pH (B).

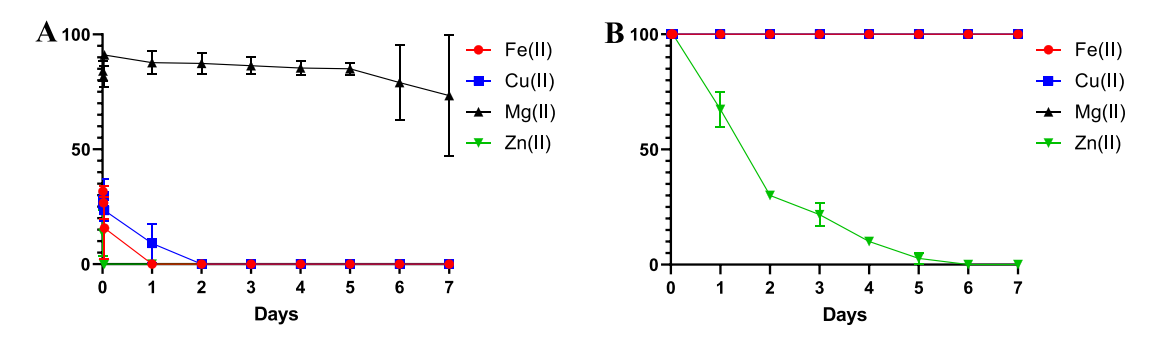


Figure 11. Stability study of [47 Sc]Sc-HOPO and [47 Sc]Sc-DOTA over the course of 7 days in the presence of metal ions. (A) [47 Sc]Sc-HOPO in the presence of 100 μ M FeCl₂, CuCl₂, MgCl₂, and ZnCl₂. (B) Stability of [47 Sc]Sc-DOTA in the presence of 100 μ M FeCl₂, CuCl₂, MgCl₂, and ZnCl₂.

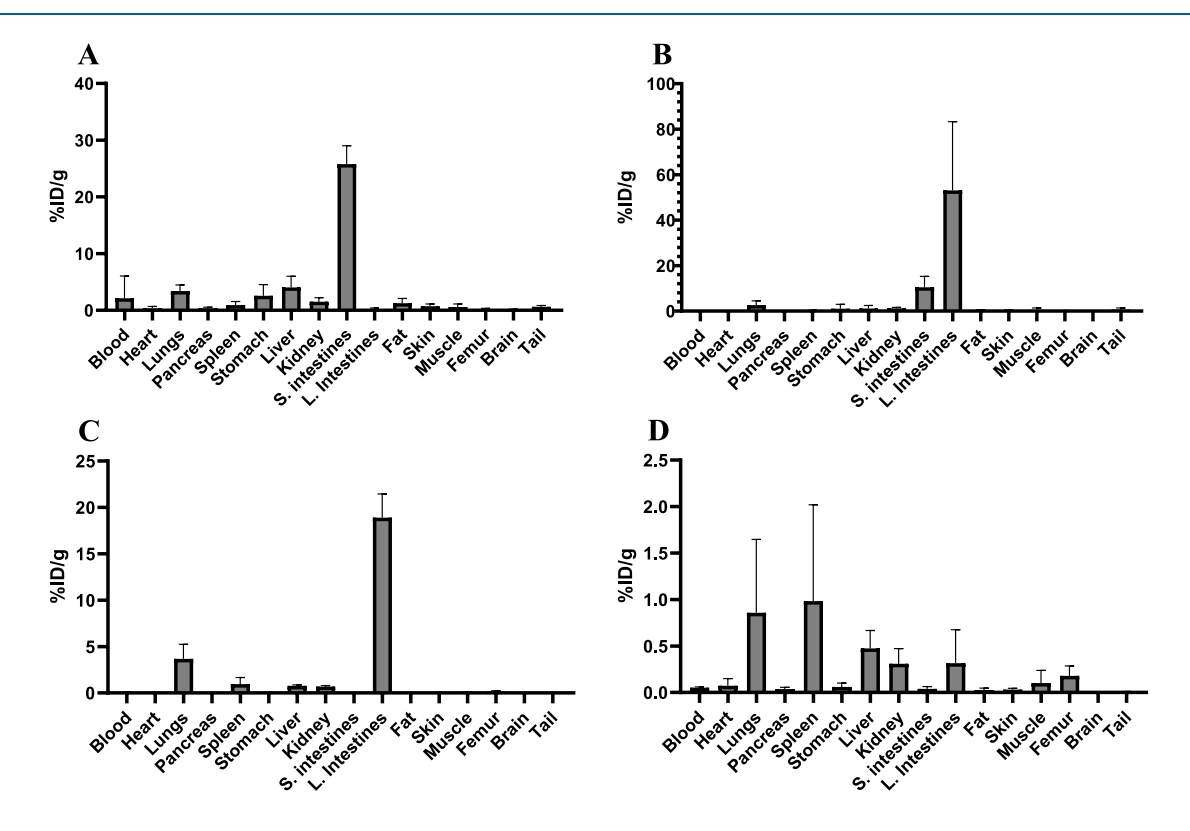


Figure 12. Biodistribution of 10 μ Ci injections of [47 Sc]Sc-HOPO in female Balb/c mice at four time points: 10 min (A); 1 h (B); 4 h (C); 24 h (D).

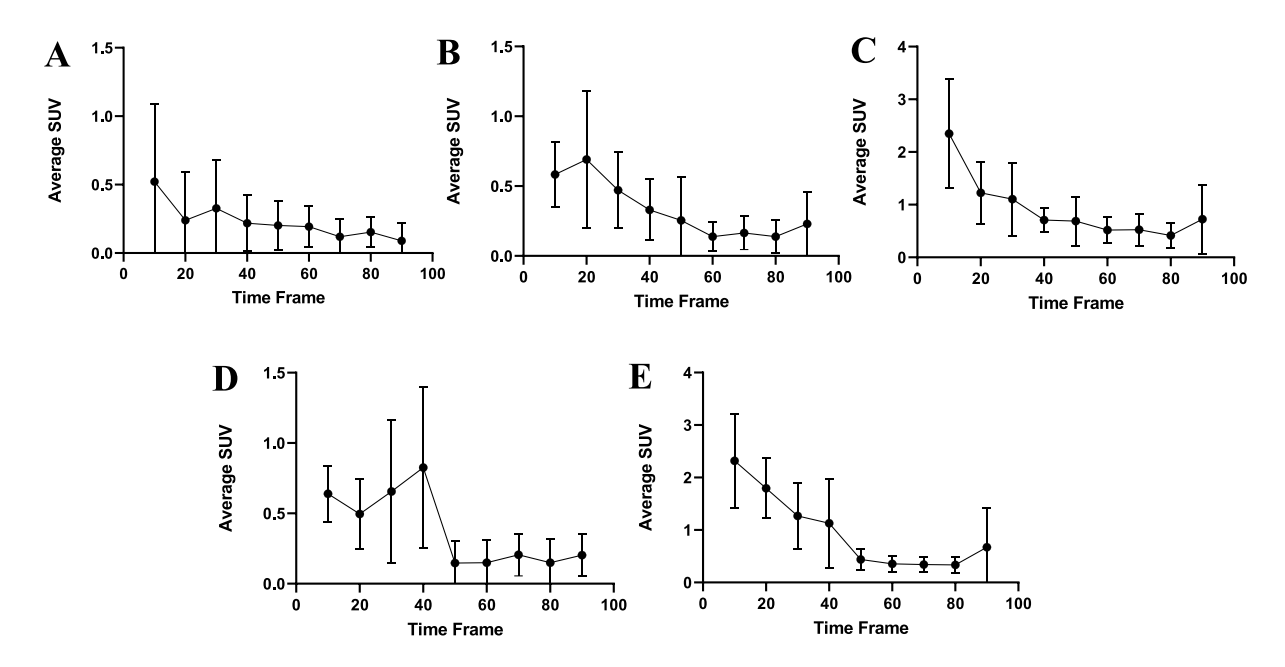


Figure 13. SUV values for various organs of 100 μ Ci of [43 Sc]Sc-HOPO taken at 10 min intervals over the course of the 90 min scan and plot of each organ to create a time activity curve for each organ: brain (A); lung (B); kidneys (C); heart (D); liver (E).

first hour and DOTA beginning to decomplex within the first day. Although DOTA outperformed HOPO in this study, this study employed relatively extreme chemical environments that are not representative of the biological conditions or the concentrations of competing metal ions that would be found there. Therefore, it is not predictive of the behavior of [⁴⁷Sc]Sc-HOPO *in vivo*. To better probe *in vivo* behavior, biodistribution studies were conducted.

Biodistribution. Four groups (n = 4) of mice were injected with 10 μ Ci of [47 Sc]Sc-HOPO, and biodistributions were performed at various time points. Figure 12 represents the average biodistribution of four mice at 10 min and 1, 4, and 24 h after injection.

The results, shown in Figure 12 and Table S3, demonstrate that $[^{47}Sc]Sc enthetact{HOPO}$ is excreted via the hepatobiliary pathway. Within the first 10 min, the complex is shown to have significant uptake in the small intestines. The 1- and 4-h biodistributions show the complex moving into large intestines. The %ID/g from the 1-h to 4-h mark also decreases, indicating that the complex is being excreted from the mouse because the other organs do not show significant uptake at both time points. Furthermore, the 24-h time point has a lower %ID/g (20% at 4 h to 2% at 24 h), indicating that the majority of the complex is largely excreted.

Another biodistribution was performed on mice injected with $[^{43}\text{Sc}]\text{Sc-HOPO}$ to further validate the biodistribution pattern and determine its suitability for PET imaging. The $[^{43}\text{Sc}]\text{Sc-HOPO}$ biodistribution data, shown in Table S4, exhibit the same trends, with the complex moving from the small intestines into the large intestines. From both biodistributions, the $[^{43,47}\text{Sc}]\text{Sc-HOPO}$ complexes show uptake and excretion through the gastrointestinal tract. Another animal study was performed with free ^{47}Sc for comparison to the biodistribution of $[^{43,47}\text{Sc}]\text{Sc-HOPO}$. Free ^{47}Sc in saline was injected into a set of mice (n=4), and the biodistribution was performed at 1 h for a direct comparison to the 1-h biodistribution time point of $[^{47}\text{Sc}]\text{Sc-HOPO}$. These

data are shown in Table S6. Free ⁴⁷Sc has a more widespread uptake within the heart, lungs, spleen, kidney, and femur. The [^{43,47}Sc]Sc-HOPO complex does not follow the same distribution path as free ⁴⁷Sc and shows uptake and excretion almost exclusively via the gastrointestinal path. This further validates the chemical inertness of [^{43,47}Sc]Sc-HOPO *in vivo*.

PET Imaging. Additional evaluation of the in vivo stability for the [43Sc]Sc-HOPO complex was determined by PET imaging in normal mice. The standard uptake value (SUV) data show a low time activity curve for the brain, lung, kidney, heart, and liver (Figure 13). The liver and kidney SUV decrease throughout the study in support of the previous data showing the complex moving through the gastrointestinal tract. The SUV data mirror the biodistribution data as the uptake for each organ was significantly lower than the intestines. Furthermore, the maximum intensity projection image of the Balb/c mice (Figure 14) clearly shows excretion through the hepatobiliary tract, and no uptake in the blood, lung, heart, kidneys, or femur was observed in the biodistribution of free ⁴⁷Sc, complimenting the biodistribution data of [⁴⁷Sc]Sc-HOPO discussed above. Both in vivo experiments show the chemical robustness of [43,47Sc]Sc-HOPO.

The data do not indicate decomplexation due to the absence of high uptake in the blood, lung, heart, and kidneys shown in both the biodistribution and dynamic images. A comparison with free 47 Sc *in vivo* was used to verify the inertness of the complex. Free 47 Sc in saline was injected into a set of mice (n = 4), and biodistribution was performed at 1 h for a direct comparison to the 1-h biodistribution of [47 Sc]Sc-HOPO. The complexes have excretion through the hepatic tract (liver and small and large intestines), while free [47 Sc]ScCl₃ has a widespread biodistribution, with uptake seen in the heart, spleen, and kidneys along with the liver and intestines, as seen in Table S5.

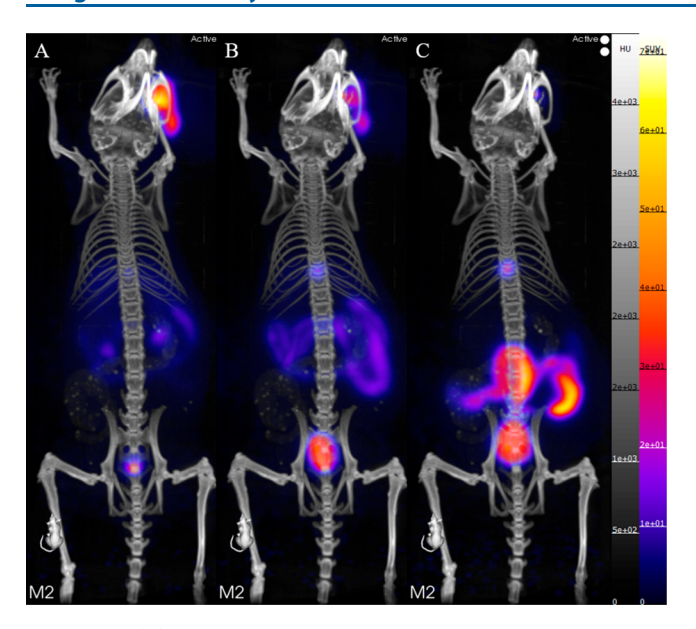


Figure 14. (A) PET/CT static image of a Balb/c mouse 0–10 min after injection of [43 Sc]Sc-HOPO. (B) PET/CT static image of a Balb/c mouse 4–50 min after injection of [43 Sc]Sc-HOPO. (C) PET/CT static image of a Balb/c mouse 80–90 min after injection of [43 Sc]Sc-HOPO. Approximately 100 μ Ci of [43 Sc]Sc-HOPO was injected.

CONCLUSIONS

The 3,4,3-(LI-1,2-HOPO) ligand has been shown to be a suitable chelator for Sc3+, and evidence presented here indicates that it is a comparable chelator to DOTA for Sc³⁺. We synthesized and characterized the macroscopic Sc-HOPO complex. The Sc-HOPO complex exhibits an expected octadentate structure with a pair of enantiomers. The Sc3+ center is bound to all eight of the coordinating O atoms from the four hydroxypyridinonate groups on the ligand. Additionally, the complex experiences a reversible protonation beginning below pH 4, as shown through pH-dependent NMR studies, observed in the HPLC and LC-MS profiles, and corroborated by DFT studies. This is consistent with the stability constant data reported by Carter et al. 40 The reversible nature of this protonation without any disruption to the complexation of Sc attests to the stability of the Sc-HOPO complex.

Radiolabeling experiments were carried out to synthesize the [43,44,47 Sc]Sc-HOPO complexes. The low p K_a values for HOPO enable it to be radiolabeled at lower pH compared to DOTA, which are more compatible with biological targeting vectors. The stability of the [43,47Sc]Sc-HOPO complexes was demonstrated by in vitro studies and in vivo biodistribution and imaging studies. The in vitro experiments demonstrate that HOPO possesses stability comparable to that of DOTA. The fast kinetics of labeling the HOPO ligand with radioscandium at mild temperatures may offer an advantage over DOTA and other macrocycles. Although acyclic chelators tend to have lower thermodynamic stability than their macrocyclic chelators, HOPO demonstrated stability that matches DOTA under the various conditions of the experiments conducted here. Furthermore, in vivo application of [43,47Sc]Sc-HOPO indicates that the complex is excreted through the intestinal tract, in contrast to the biodistribution of free ⁴⁷Sc, where there is significant uptake in the heart, lungs, spleen, kidneys, and femur. Accordingly, there is no indication of decomplexation of [^{43,47}Sc]Sc-HOPO. Overall, this study demonstrates the viability of the Sc-HOPO complex as a potential construct for radioscandium-based agents and paves the way for future work with bifunctional HOPO variants for targeted imaging and therapy.

EXPERIMENTAL SECTION

Materials and Methods. All radioactive work was done in laboratories approved to handle low levels of radioactivity for γ and β emitters with appropriate safety training and radiation monitoring. All chemicals were purchased from Fisher or Sigma-Aldrich and used without purification. All water was ultrapure (>18.2 M Ω). Instruments were calibrated and maintained according to standard quality control procedures. Compounds were analyzed by liquid chromatography-high-resolution mass spectrometry (LC-HRMS). LC-HRMS was performed on an Agilent 6550 iFunnel Q-TOF mass spectrometer coupled to an Agilent 1290 Infinity LC system (binary pump, diode-array detector, and autosampler). Chromatography was performed using an Agilent SB-C8 column (2.1 × 50 mm) at 45 °C and a gradient of solvents A (water, 0.1% formic acid) and B (acetonitrile, 0.1% formic acid) from 2 to 98% solvent B in 10 min at a flow rate of 0.2 mL/min. The following settings were applied to the electrospray ionization (ESI) source: gas temperature, 250 °C; nebulizer, 30 psig; sheath gas temperature, 250 °C; Vcap, 3500 V; nozzle voltage, 2000 V. For MS analysis, full-scan mass spectra (m/z)100-3000) were acquired in positive-ion mode. Data were acquired and analyzed using Agilent's MassHunter Software suite (Data Acquisition B.09.00, Qualitative Analysis B.07.00). ¹H NMR experiments were performed on a Bruker Avance III 600 MHz NMR spectrometer with data processed by Topspin 4.1.4 software. 45Sc NMR experiments were performed on a Bruker Avance III 400 MHz NMR spectrometer. NMR spectra are expressed on the δ scale. NMR spectra were referenced to solvent peaks or 3-(trimethylsilyl)-1propanesulfonic acid, sodium salt (DSS). Measurement of the pH was performed on a Fisherbrand Accument AE150 pH meter with a Fisherbrand Accumet Micro Glass Mercury-Free Combination Electrode. The HPLC system used for analysis and purification of a macroscopic material was a Shimadzu Prominence system equipped with a diode array and an automatic fraction collector. HPLC purification was performed with a Shimadzu GIST Shim Packed C18 Semipreparative 10 × 250 mm column, and analysis was performed on a Kromasil Universal C18 4.6 × 250 mm column. UV-vis spectroscopy was performed on a Thermo Evolution 220 UV-vis spectrophotometer. Infrared attenuated total reflectance (IR-ATR) spectroscopy was performed on a PerkinElmer Spectrum 2 FT-IR spectrometer with a Universal ATR sampling accessory. X-ray diffraction data were collected on a Bruker X8 Kappa Apex II diffractometer using Mo K α radiation. ⁴⁴Sc was obtained at BNL from a $^{44}\mathrm{Ti}/^{44}\mathrm{Sc}$ generator. Enriched $[^{46,50}\mathrm{Ti}]\mathrm{TiO}_2$ was obtained from the Department of Energy. Proton irradiations were performed on TR-24 cyclotron [Advanced Cyclotron Systems (ACSI, Inc.)]. Activity measurements were performed on a Canberra S5000 high-purity germanium (HPGe) and analyzed with the Canberra Genie 2000 software. The energy and efficiency calibration for the HPGe was performed using a mixed nuclide sealed source from Eckert and Ziegler Analytics. Radio-TLC was performed on ITLC-SG plates purchased from Agilent Technologies (Santa Clara, CA) and measured on an Eckert and Ziegler AR-2000 and processed using Winscan Radio-TLC software (Eckert and Zeigler, AR2000, Windscan software, Berlin, Germany). The HPLC system used for ⁴³Sc and ⁴⁷Sc work was an Agilent Technologies 1260 Infinity high-performance liquid chromatograph with UV and radioactivity detectors and a Xterra MS packed C18 4.6 × 150 mm column from Waters. A purity of >95% was confirmed using quantitative HPLC analysis for nonradioactive compounds and radio-TLC for radioactive compounds. The tissue weight and radioactivity was measured via an automated gamma counter (Hidex AMG, Turku, Finland). PET/CT images were acquired using a Sofie GNEXT PET/CT scanner (Sofie Biosciences, Gilroy, CA).

3,4,3-(LI-1,2-HOPO). The ligand was synthesized as previously described with slight modification. ^{24,32,33} Purification of the final compound was performed using HPLC. Details are presented in the Supporting Information.

Sc-HOPO. A solution of scandium chloride (ScCl₃·6H₂O) (9 mg, 34.7 μ mol) in water (5 mL) was added to a solution of HOPO (25 mg, 33.3 μ mol) in water (5 mL). The mixture was shaken on a thermomixer at RT for 15 min. The resulting solution was cloudy with a white precipitate, and a pH of 3.5. A solution of 2 M K₂CO₃ was used to provide a K⁺ counterion to the Sc(HOPO)⁻ complex and to solubilize the product. At pH 7-8, the precipitate dissolved into a solution with heat and did not precipitate upon cooling. The solution was filtered, lyophilized, redissolved in water, and purified by HPLC [H₂O/acetonitrile (ACN) + 0.1% 2,2,2-trifluoroacetic acid (TFA), 15–25% ACN over 15 min]. NMR was performed in D₂O adjusted to pH 7 with K₂CO₃ to improve solubility. Variable-pH ¹H NMR and ⁴⁵Sc NMR experiments used K₂CO₃ and DCl to adjust the pH. UV– vis characterization was attempted but was not conclusive. The complex was also characterized by IR-ATR spectroscopy, HRMS, and X-ray crystallography. More details on these methods are presented in the Supporting Information.

Radiolabeling Studies. ⁴⁴Sc was received as [44 Sc]ScCl₃ in 2.0 M HCl by elution from a 44 Ti/ 44 Sc generator. This solution was heated to dryness and then treated with 0.1 M HNO₃ and 30% H₂O₂ to destroy contaminants left from the elution. This was dried down, and 44 Sc was reconstituted in 0.5–1.0 mL of 0.1 M HCl. HOPO and DOTA were labeled at various concentrations (5–250 μ M) in water with 100 mM ammonium acetate at pH 5. Radiolabeling times varied from 5 to 60 min. Radiolabeling experiments were carried out at RT, 37 °C, and 95 °C, with pH values ranging from 1 to 8. Radiolabeling reactions were performed with activity ranging from 5 μ Ci to 1 mCi. Reactions were monitored via radio-TLC using ITLC-SG strips and 50 mM EDTA at pH 5 as the mobile phase. [44 Sc]Sc ligand complexes move with R_f = 0.2, while free 44 Sc was complexed by EDTA and moved with the solvent front.

 43,47 Sc was produced via proton bombardment on enriched $[^{46,50}\text{Ti}]$ TiO $_2$, respectively. After bombardment, $[^{50}\text{Ti}]$ TiO $_2$ was dissolved using a 3:1 mass ratio of NH₄HF₂ at 250 °C and brought into solution with 5 mL of concentrated HCl. The solution was diluted to 10.5 M HCl before addition to a 150 mg of preconditioned branched N,N,N',N'-tetra-n-octyldiglcolamide resin. The column was rinsed with 9 M HCl, 7 M HNO₃, and 1 M HNO₃ before ^{43,47}Sc was eluted in 0.1 M HCl. The collected ⁴⁷Sc was dried down and redissolved in 200 µL 0.25 M ammonium acetate (pH 4). For HOPO, 260 μ Ci of ⁴⁷Sc was used for labeling in a 194 μ L solution with 0.21 mM HOPO, pH 8, at 37 $^{\circ}\text{C}$, 800 rpm for 30 min with an apparent molar activity of 6.4 mCi/ μ mol of [47 Sc]Sc-HOPO. For DOTA, 260 μ Ci of ⁴⁷Sc was used for labeling in a final volume of 145 μ L with a final concentration of 0.21 mM DOTA, pH 4, at 95 °C for 30 min with an apparent molar activity of 8.5 mCi/ μ mol of [47 Sc]Sc-DOTA. Radiolabeling was verified by ITLC-SG strips developed in 50 mM EDTA. Free ⁴⁷Sc moved with the solvent front while the labeled complex had $R_f = 0.65$.

DFT Calculations. All calculations were based on DFT within the B3LYP approximation. 44 For the Sc atom, the lanl2tz(f) basis set was used, 45 whereas all nontransition metals were represented with the 6-311G+(d,p) basis set.⁴⁶ For all systems, the lowest-energy structure was obtained by doing a full geometry optimization. A harmonic vibrational analysis was performed on the optimized structures to ensure that a minimum was located and to obtain the thermodynamic properties. Calculations were performed in the vapor phase and in solution using the conductor-like polarizable continuum model (CPCM) for water. 47 All calculations were performed using Gaussian 09.48 The crystal structure obtained experimentally for the Sc-(HOPO)⁻¹ (8-coordinate complex) was used as the initial structure in the optimization procedure. The 7-coordinate complexes were generated by adding a proton to the outer (called 7-coordinate B) or inner (called 7-coordinate C) oxygen in the hydroxypyridinonate group. The stability of the 8- and 7-coordinate complexes was computed for the following reactions:

$$HOPO^{4-} + Sc(H_2O)_6^{3+} \rightarrow Sc(HOPO)^- + 6H_2O$$
 (Rxn 1)

$$Sc(HOPO)^- + H_3O^+$$

$$\rightarrow$$
 Sc(HOPOH) + H₂O 7-coordinate A

$$\rightarrow$$
 Sc(HOPOH) + H₂O 7-coordinate B (Rxn 2)

The change in te Gibbs free energy for these reactions in the vapor were obtained from

$$\Delta G_{\text{Rx1}}^{\text{v}} = G_{\text{Sc(HOPO)}^{-}}^{\text{v}} + 6G_{\text{H}_{2}\text{O}}^{\text{v}} - G_{(\text{HOPO)}^{4-}}^{\text{v}} - G_{\text{Sc(H}_{2}\text{O})^{3+}}^{\text{v}}$$
(1)

$$\Delta G_{\text{Rx2}}^{\text{v}} = G_{\text{Sc(HOPOH)}}^{\text{v}} - G_{\text{Sc(HOPO)}^{-}}^{\text{v}} - G_{(\text{H}_{2}\text{O})^{+}}^{\text{v}}$$
(2)

To obtain the change in the Gibbs free energy in solution, a thermodynamic cycle ^{49,50} (Figure 15) was used such that

$$\Delta G_{\text{Rx1 or Rx2}}^{\text{s}} = \Delta G_{\text{Rx1 or Rx2}}^{\text{v}} + \sum_{i=1}^{M} \Delta G_{i}^{\text{solvation}} - \sum_{i=1}^{N} \Delta G_{i}^{\text{solvation}}$$
(3)

$$\begin{array}{cccc} & \Delta G_{sol} \\ A_{sol} + B_{sol} & \longrightarrow & AB_{sol} \\ \Delta G_{desolvation} & & & & & \Delta G_{solvation} \\ & & & & & & & \Delta G_{solvation} \\ & & & & & & & & \Delta G_{vap} \end{array}$$

$$\Delta G_{sol} = \Delta G_{desolvation} + \Delta G_{vap} + \Delta G_{solvation}$$

$$\Delta G_{desolvation} > 0$$
 $\Delta G_{solvation} < 0$ $\Delta G_{vapor} < 0$

Figure 15. General thermodynamics cycle used to calculate the change in the thermodynamic properties in solution.

where M and N are the total number of reactant and product molecules, respectively, and $\Delta G_{\text{solvation}}^i$ is the change in the Gibbs free energy of solvation of species i. A similar cycle was used to obtain changes in the enthalpy in solution. The change in the entropy was obtained from $\Delta S = \frac{\Delta H - \Delta G}{T}$. All thermodynamic quantities are reported at T=300 K. Additionally, the change in the electronic energy for both Rxn 1 and Rxn 2 were obtained using the DFT/B3LYP/6-311G+(d,p) energy obtained after minimization.

Stability Studies. For each stability study (EDTA challenge study or metal challenge study), a vial of 120 μ Ci of [47 Sc]Sc-DOTA or [47 Sc]Sc-HOPO from the stock solution was diluted to 1200 μ L with Chelex water.

EDTA Challenge Study. An EDTA challenge was performed at varying pH of 5, 6, 7, and 8. Each pH challenge was done in triplicate. Each vial contained 100 μ L of the stock solution of either [47 Sc]Sc-DOTA or [47 Sc]Sc-HOPO for an average of 10 μ Ci. A total of 50 μ L of EDTA was added to the solution and diluted to 500 μ L with Chelex purified water for a final concentration of 10 μ M ligand and 100 μ M EDTA. Solutions were assessed via ITLC at 15 min, 30 min, 1 h, and then daily time points up to 7 days. Solutions were kept at 37 °C with agitation throughout this study.

Metal Challenge Study. A metal challenge was performed with FeCl₂, CuCl₂, MgCl₂, and ZnCl₂ in triplicate. Each vial contained 100 μ L of the stock solution of either [47 Sc]Sc-DOTA or [47 Sc]Sc-HOPO for an average of 10 μ Ci. A total of 50 μ L of the metal solution was added to the solution and then diluted to 500 μ L with Chelex purified water for a final concentration of 10 μ M ligand and 100 μ M metal. Solutions were assessed via ITLC at 15 min, 30 min, 1 h, and then daily time points up to 7 days. Solutions were kept at 37 °C with agitation throughout this study.

PET Imaging and Biodistribution. HOPO was radiolabeled with either ⁴³Sc or ⁴⁷Sc in yields of >96%, at 37 °C and pH 8 for 30 min as described above. The dose was diluted with a 0.9% NaCl solution to achieve 100 μ L injections: 10 μ Ci injections of [47 Sc]Sc-HOPO (apparent molar activity of 8.4 mCi/ μ mol for the stock dose) and 100 μ Ci of [43Sc]Sc-HOPO (apparent molar activity of 12.4 mCi/ μ mol for the stock dose). The radiolabeled doses did not require purification prior to injection. Longer-term biodistributions were analyzed with [47Sc]Sc-HOPO for four time points: 10 min and 1, 4, and 24 h. At each time point, mice (n = 4) were sacrificed and the radioactivity was assessed in the following organs: 50 μ L of blood, heart, lung, liver, spleen, pancreas, stomach, kidneys, small intestine, large intestine, fat, skin, muscle, femur, brain, and tail. Each sample was added to a preweighed vial. The vials were weighed and counted on a γ counter, and the percentage of injected dose per gram of tissue was calculated.

PET (energy window 350-650 keV) and computed tomography (CT; voltage 80 kVp, current 150 μ A, 720 projections, scan time 5 min) imaging was performed immediately after retroorbital injection of 100 μ Ci of [43Sc]Sc-HOPO. The PET data were collected for 90 min of dynamic imaging, followed by 5 min of CT. Following imaging, biodistribution was conducted as described above. PET images were reconstructed via the 3D-OSEM (Ordered Subset Expectation Maximization) algorithm (24 subsets and 3 iterations) with random, attenuation, and decay correction, and CT was reconstructed with the Modified Feldkamp Algorithm and analyzed using VivoQuant 4.0 (Invicro Imaging Service and Software, Boston MA) software. After the images were reconstructed, the PET images were appended to the CT images. Following image reconstruction, regions of interest were drawn for select tissues (brain, lung, liver, kidneys, and muscle) in each mouse based on the CT images for each frame. The time-activity curves of the uptake of the tracer were generated over the course of data collection.

ASSOCIATED CONTENT

Supporting Information

The Supporting Information is available free of charge at https://pubs.acs.org/doi/10.1021/acs.inorgchem.2c03931.

Experimental details for the synthesis of HOPO and additional characterization of the HOPO ligand and macroscopic Sc-HOPO, which includes ⁴⁴Sc radio-labeling data, tabulated biodistribution data, and a GIF version of the dynamic PET image of [⁴³Sc]Sc-HOPO in healthy mice (PDF)

PET/CT video image of a Balb/c mouse (AVI)

Accession Codes

CCDC 2217080 contains the supplementary crystallographic data for this paper. These data can be obtained free of charge via www.ccdc.cam.ac.uk/data_request/cif, or by emailing data_request@ccdc.cam.ac.uk, or by contacting The Cambridge Crystallographic Data Centre, 12 Union Road, Cambridge CB2 1EZ, UK; fax: +44 1223 336033.

AUTHOR INFORMATION

Corresponding Author

Melissa A. Deri — Ph.D. Program in Chemistry, The Graduate Center of the City University of New York, New York, New York 10016, United States; Department of Chemistry, Lehman College of the City University of New York, Bronx, New York 10468, United States; ◎ orcid.org/0000-0003-4186-5572; Email: melissa.deri@lehman.cuny.edu

Authors

Michael D. Phipps – Ph.D. Program in Chemistry, The Graduate Center of the City University of New York, New York, New York 10016, United States; Department of

- Chemistry, City University of New York Hunter College, New York, New York 10065, United States; Department of Chemistry, Lehman College of the City University of New York, Bronx, New York 10468, United States; Program in Molecular Pharmacology and Chemistry, Memorial Sloan Kettering Cancer Center, New York, New York 10065, United States
- Shelbie Cingoranelli Department of Radiology, University of Alabama at Birmingham (UAB), Birmingham, Alabama 35294, United States
- N. V. S. Dinesh K. Bhupathiraju Department of Chemistry, City University of New York Hunter College, New York, New York 10065, United States; orcid.org/0000-0002-5885-3722
- Ali Younes Department of Chemistry, City University of New York Hunter College, New York, New York 10065, United States; orcid.org/0000-0001-7351-2726
- Minhua Cao Department of Chemistry, City University of New York Hunter College, New York, New York 10065, United States
- Vanessa A. Sanders Medical Isotope Research and Production Laboratory, Collider–Accelerator Division, Brookhaven National Laboratory (BNL), Upton, New York 11973, United States
- Michelle C. Neary Department of Chemistry, City University of New York Hunter College, New York, New York 10065, United States; orcid.org/0000-0003-2805-3668
- Matthew H. Devany Department of Chemistry, City University of New York Hunter College, New York, New York 10065, United States
- Cathy S. Cutler Medical Isotope Research and Production Laboratory, Collider–Accelerator Division, Brookhaven National Laboratory (BNL), Upton, New York 11973, United States
- Gustavo E. Lopez Ph.D. Program in Chemistry, The Graduate Center of the City University of New York, New York, New York 10016, United States; Department of Chemistry, Lehman College of the City University of New York, Bronx, New York 10468, United States; orcid.org/0000-0003-1660-547X
- Shefali Saini Department of Radiology, University of Alabama at Birmingham (UAB), Birmingham, Alabama 35294, United States
- Candace C. Parker Department of Radiology, University of Alabama at Birmingham (UAB), Birmingham, Alabama 35294, United States; Occid.org/0000-0001-6744-7438
- Solana R. Fernandez Department of Radiology, University of Alabama at Birmingham (UAB), Birmingham, Alabama 35294, United States
- Jason S. Lewis Program in Molecular Pharmacology and Chemistry, Memorial Sloan Kettering Cancer Center, New York, New York 10065, United States; ⊚ orcid.org/0000-0001-7065-4534
- Suzanne E. Lapi Department of Radiology, University of Alabama at Birmingham (UAB), Birmingham, Alabama 35294, United States
- Lynn C. Francesconi Ph.D. Program in Chemistry, The Graduate Center of the City University of New York, New York, New York 10016, United States; Department of Chemistry, City University of New York Hunter College, New York, New York 10065, United States; orcid.org/0000-0001-6314-2899

Complete contact information is available at: https://pubs.acs.org/10.1021/acs.inorgchem.2c03931

Author Contributions

[†]M.D.P. and S.C. contributed equally to this work.

Notes

The authors declare the following competing financial interest(s): A patent on the bifunctional p-SCN-Bn-HOPO chelator has been filed with J.S.L., L.C.F, and M.A.D. as inventors.

ACKNOWLEDGMENTS

The authors thank the Medical Isotopes Research and Production Group at BNL for providing the 44Sc used in this paper through the support of DOE IP# ST5001020 (to C.S.C.). The authors also acknowledge the NSF-IGERT Program NSF-DGE 0965983 (to L.C.F.), The Tow Foundation Graduate Fellowship from the MSKCC Center for Molecular Imaging and Nanotechnology (to M.D.P.), and CUNY Hunter College for their support of this research. The authors also thank Hunter Mass Spectrometry. Research reported in this publication was supported by the National Institute of General Medical Sciences of the National Institutes of Health under Award SC2GM130464 (to M.A.D.). The content is solely the responsibility of the authors and does not necessarily represent the official views of the National Institutes of Health. The MSK Radiochemistry and Molecular Imaging Probes Core Facility and the MSK Small Animal Imaging Facility were supported in part by NIH P30 CA08748. This study was also supported in part by NIH R35 CA232130-01A1 (to J.S.L.). The production of ⁴³Sc and ⁴⁷Sc was supported by the Department of Energy Isotope Program under Grant DESC0020197 (to S.E.L.). Small animal imaging studies were supported by the O'Neal Comprehensive Cancer Center at UAB through Grant P30CA013148.

REFERENCES

- (1) FDA-approved radiopharmaceuticals 2022. https://www.cardinalhealth.com/content/dam/corp/web/documents/fact-sheet/cardinal-health-fda-approved-radiopharmaceuticals.pdf (accessed 10/19/2022).
- (2) Information extracted from the NuDat Database, National Nuclear Data Center, 2021.
- (3) Müller, C.; Bunka, M.; Haller, S.; Köster, U.; Groehn, V.; Bernhardt, P.; van der Meulen, N.; Türler, A.; Schibli, R. Promising Prospects for 44Sc-/47Sc-Based Theragnostics: Application of 47Sc for Radionuclide Tumor Therapy in Mice. *J. Nucl. Med.* **2014**, *55* (10), 1658–1664.
- (4) Kerdjoudj, R.; Pniok, M.; Alliot, C.; Kubicek, V.; Havlickova, J.; Rosch, F.; Hermann, P.; Huclier-Markai, S. Scandium(iii) complexes of monophosphorus acid DOTA analogues: a thermodynamic and radiolabelling study with 44Sc from cyclotron and from a 44Ti/44Sc generator. *Dalton Trans.* **2016**, *45* (4), 1398–1409.
- (5) Domnanich, K. A.; Müller, C.; Farkas, R.; Schmid, R. M.; Ponsard, B.; Schibli, R.; Türler, A.; van der Meulen, N. P. (44)Sc for labeling of DOTA- and NODAGA-functionalized peptides: preclinical in vitro and in vivo investigations. *EJNMMI Radiopharm. Chem.* **2017**, *1* (1), 8–8.
- (6) Eppard, E.; de la Fuente, A.; Benešová, M.; Khawar, A.; Bundschuh, R. A.; Gärtner, F. C.; Kreppel, B.; Kopka, K.; Essler, M.; Rösch, F. Clinical Translation and First In-Human Use of [(44)Sc]Sc-PSMA-617 for PET Imaging of Metastasized Castrate-Resistant Prostate Cancer. *Theranostics* **2017**, *7* (18), 4359–4369.
- (7) Umbricht, C. A.; Benesova, M.; Schmid, R. M.; Turler, A.; Schibli, R.; van der Meulen, N. P.; Muller, C. (44)Sc-PSMA-617 for

- radiotheragnostics in tandem with (177)Lu-PSMA-617-preclinical investigations in comparison with (68)Ga-PSMA-11 and (68)Ga-PSMA-617. *EJNMMI Res.* **2017**, 7 (1), 9.
- (8) Edem, P. E.; Sinnes, J. P.; Pektor, S.; Bausbacher, N.; Rossin, R.; Yazdani, A.; Miederer, M.; Kjaer, A.; Valliant, J. F.; Robillard, M. S.; Rosch, F.; Herth, M. M.Evaluation of the inverse electron demand Diels-Alder reaction in rats using a scandium-44-labelled tetrazine for pretargeted PET imaging. *EJNMMI Res.***2019**, 9. DOI: 10.1186/s13550-019-0520-y
- (9) Siwowska, K.; Guzik, P.; Domnanich, K. A.; Monné Rodríguez, J. M.; Bernhardt, P.; Ponsard, B.; Hasler, R.; Borgna, F.; Schibli, R.; Köster, U.; van der Meulen, N. P.; Müller, C. Therapeutic Potential of (47)Sc in Comparison to (177)Lu and (90)Y: Preclinical Investigations. *Pharmaceutics* **2019**, *11* (8), 424.
- (10) Hernandez, R.; Valdovinos, H. F.; Yang, Y.; Chakravarty, R.; Hong, H.; Barnhart, T. E.; Cai, W. 44Sc: An Attractive Isotope for Peptide-Based PET Imaging. *Mol. Pharmaceutics* **2014**, *11* (8), 2954–2961.
- (11) Honarvar, H.; Müller, C.; Cohrs, S.; Haller, S.; Westerlund, K.; Karlström, A. E.; van der Meulen, N. P.; Schibli, R.; Tolmachev, V. M. Evaluation of the first 44Sc-labeled Affibody molecule for imaging of HER2-expressing tumors. *Nuclear medicine and biology* **2017**, *45*, 15–21
- (12) Price, E. W.; Orvig, C. Matching chelators to radiometals for radiopharmaceuticals. *Chem. Soc. Rev.* **2014**, 43 (1), 260–90.
- (13) Zeglis, B. M.; Houghton, J. L.; Evans, M. J.; Viola-Villegas, N.; Lewis, J. S. Underscoring the influence of inorganic chemistry on nuclear imaging with radiometals. *Inorg. Chem.* **2014**, *53* (4), 1880–99
- (14) Walczak, R.; Gawęda, W.; Dudek, J.; Choiński, J.; Bilewicz, A. Influence of metal ions on the 44Sc-labeling of DOTATATE. J. Radioanal. Nucl. Chem. 2019, 322 (2), 249–254.
- (15) Eppard, E.; De la Fuente, A.; Benesova, M.; Khawar, A.; Bundschuh, R. A.; Gartner, F. C.; Kreppel, B.; Kopka, K.; Essler, M.; Rosch, F. Clinical Translation and First In-Human Use of [44Sc]Sc-PSMA-617 for PET Imaging of Metastasized Castrate-Resistant Prostate Cancer. *Theranostics* **2017**, *7*, 4359.
- (16) Połosak, M.; Piotrowska, A.; Krajewski, S.; Bilewicz, A. Stability of 47Sc-complexes with acyclic polyamino-polycarboxylate ligands. *J. Radioanal. Nucl. Chem.* **2013**, 295 (3), 1867–1872.
- (17) Huclier-Markai, S.; Alliot, C.; Sebti, J.; Brunel, B.; Aupiais, J. A comparative thermodynamic study of the formation of scandium complexes with DTPA and DOTA. *RSC Adv.* **2015**, *5* (121), 99606–99617.
- (18) Huclier-Markai, S.; Sabatie, A.; Ribet, S.; Kubicek, V.; Paris, M.; Vidaud, C.; Hermann, P.; Cutler, C. S. Chemical and biological evaluation of scandium(III)-polyaminopolycarboxylate complexes as potential PET agents and radiopharmaceuticals. *Radiochim. Acta* **2011**, 99 (10), 653–662.
- (19) Sinnes, J. P.; Nagel, J.; Rosch, F. AAZTA(5)/AAZTA(5)-TOC: synthesis and radiochemical evaluation with (68)Ga, (44)Sc and (177)Lu. *EJNMMI Radiopharm. Chem.* **2019**, *4* (1), 18.
- (20) Vaughn, B. A.; Ahn, S. H.; Aluicio-Sarduy, E.; Devaraj, J.; Olson, A. P.; Engle, J.; Boros, E. Chelation with a twist: a bifunctional chelator to enable room temperature radiolabeling and targeted PET imaging with scandium-44. *Chemical Science* **2020**, *11* (2), 333–342.
- (21) Chakravarty, R.; Goel, S.; Valdovinos, H. F.; Hernandez, R.; Hong, H.; Nickles, R. J.; Cai, W. Matching the decay half-life with the biological half-life: ImmunoPET imaging with (44)Sc-labeled cetuximab Fab fragment. *Bioconjug Chem.* **2014**, *25* (12), 2197–204.
- (22) Daumann, L. J.; Tatum, D. S.; Snyder, B. E. R.; Ni, C.; Law, G.-l.; Solomon, E. I.; Raymond, K. N. New Insights into Structure and Luminescence of EuIII and SmIII Complexes of the 3,4,3-LI(1,2-HOPO) Ligand. J. Am. Chem. Soc. 2015, 137, 2816–2819.
- (23) Deri, M. A.; Ponnala, S.; Kozlowski, P.; Burton-Pye, B. P.; Cicek, H. T.; Hu, C.; Lewis, J. S.; Francesconi, L. C. p-SCN-Bn-HOPO: A Superior Bifunctional Chelator for 89Zr ImmunoPET. *Bioconjugate Chem.* **2015**, *26* (12), 2579–2591.

- (24) Deri, M. A.; Ponnala, S.; Zeglis, B. M.; Pohl, G.; Dannenberg, J. J.; Lewis, J. S.; Francesconi, L. C. Alternative Chelator for 89Zr Radiopharmaceuticals: Radiolabeling and Evaluation of 3,4,3-(LI-1,2-HOPO). *J. Med. Chem.* **2014**, 57 (11), 4849–4860.
- (25) An, D. D.; Kullgren, B.; Jarvis, E. E.; Abergel, R. J. From early prophylaxis to delayed treatment: Establishing the plutonium decorporation activity window of hydroxypyridinonate chelating agents. *Chemico-Biological Interactions* **2017**, 267, 80–88.
- (26) Deblonde, G. J.-P.; Ricano, A.; Abergel, R. J. Ultra-selective ligand-driven separation of strategic actinides. *Nat. Commun.* **2019**, *10* (2438), 1–9.
- (27) Migliorati, V.; D'Angelo, P. Unraveling the Sc3+ Hydration Geometry: The Strange Case of the Far-Coordinated Water Molecule. *Inorg. Chem.* **2016**, *55* (13), 6703–6711.
- (28) Sears, J. M.; Boyle, T. J. Structural properties of scandium inorganic salts. *Coord. Chem. Rev.* **2017**, 340, 154–171.
- (29) Gao, S.-M.; Guo, W.-P.; Jin, L.; Ding, Y.-H. Maximum Carbonyl-Coordination Number of Scandium Computational Study of Sc(CO)n (n 5 1–7), Sc(CO)7 and Sc(CO)6 3-. *Int. J. Quantum Chem.* **2013**, *113*, 1192–1199.
- (30) Bhupathiraju, N. V. S. D. K.; Younes, A.; Cao, M.; Ali, J.; Cicek, H. T.; Tully, K. M.; Ponnala, S.; Babich, J. W.; Deri, M. A.; Lewis, J. S.; Francesconi, L. C.; Drain, C. M. Improved synthesis of the bifunctional chelator p-SCN-Bn-HOPO. *Organic & Biomolecular Chemistry* **2019**, *17* (28), 6866–6871.
- (31) Shannon, R. D. Revised Effective Ionic Radii and Systematic Studies of Interatomie Distances in Halides and Chaleogenides. *Acta Crystallogr. Sect. A: Found. Crystallogr.* 1976, 32, 751–767.
- (32) Xu, J.; Durbin, P. W.; Kullgren, B.; Ebbe, S. N.; Uhlir, L. C.; Raymond, K. N. Synthesis and Initial Evaluation for In Vivo Chelation of Pu(IV) of a Mixed Octadentate Spermine-Based Ligand Containing 4-Carbamoyl-3-hydroxy-1-methyl-2(1H)-pyridinone and 6-Carbamoyl-1-hydroxy-2(1H)-pyridinone. *J. Med. Chem.* **2002**, 45 (18), 3963–3971.
- (33) Fritsch, P.; Herbreteau, D.; Moutairou, K.; Lantenois, G.; Richard-le Naour, H.; Grillon, G.; Hoffschir, D.; Poncy, J. L.; Laurent, A.; Masse, R. Comparative Toxicity of 3,4,3-LIHOPO and DTPA in Baboons: Preliminary Results. *Radiation Protection Dosimetry* **1994**, 53 (1–4), 315–318.
- (34) Abergel, R. J.; Durbin, P. W.; Kullgren, B.; Ebbe, S. N.; Xu, J.; Chang, P. Y.; Bunin, D. I.; Blakely, E. A.; Bjornstad, K. A.; Rosen, C. J.; Shuh, D. K.; Raymond, K. N. Biomimetic actinide chelators: an update on the preclinical development of the orally active hydroxypyridonate decorporation agents 3,4,3-LI(1,2-HOPO) and 5-LIO(Me-3,2-HOPO). *Health Phys.* 2010, 99 (3), 401–7.
- (35) Pniok, M.; Kubiček, V.; Havličková, J.; Kotek, J.; Sabatie-Gogová, A.; Plutnar, J.; Huclier-Markai, S.; Hermann, P. Thermodynamic and Kinetic Study of Scandium(III) Complexes of DTPA and DOTA: A Step Toward Scandium Radiopharmaceuticals. *Chem. Eur. J.* 2014, 20 (26), 7944–7955.
- (36) Nagy, G.; Szikra, D.; Trencsényi, G.; Fekete, A.; Garai, I.; Giani, A. M.; Negri, R.; Masciocchi, N.; Maiocchi, A.; Uggeri, F.; Tóth, I.; Aime, S.; Giovenzana, G. B.; Baranyai, Z. AAZTA: An Ideal Chelating Agent for the Development of 44Sc PET Imaging Agents. *Angew. Chem., Int. Ed.* **2017**, 56 (8), 2118–2122.
- (37) Rehder, D.; Speh, M. An exploratory scandium-45 NMR study into the complexation of alanine and oligopeptides. *Inorg. Chim. Acta* **1987**, *135* (1), *73*–*79*.
- (38) Rehder, D.; Hink, K. The interaction of Sc(OH)2+·aq with serine and small peptides investigated by 45Sc NMR spectroscopy. *Inorg. Chim. Acta* **1989**, 158 (2), 265–271.
- (39) Nonat, A. M.; Gateau, C.; Fries, P. H.; Helm, L.; Mazzanti, M. New Bisaqua Picolinate-Based Gadolinium Complexes as MRI Contrast Agents with Substantial High-Field Relaxivities. *Eur. J. Inorg. Chem.* **2012**, 2012 (12), 2049–2061.
- (40) Carter, K. P.; Deblonde, G. J. P.; Lohrey, T. D.; Bailey, T. A.; An, D. D.; Shield, K. M.; Lukens, W. W.; Abergel, R. J. Developing scandium and yttrium coordination chemistry to advance theranostic radiopharmaceuticals. *Commun. Chem.* **2020**, *3* (1), 61.

- (41) Aihara, J.-i. Reduced HOMO-LUMO Gap as an Index of Kinetic Stability for Polycyclic Aromatic Hydrocarbons. *J. Phys. Chem.* A **1999**, *103* (37), 7487–7495.
- (42) Miar, M.; Shiroudi, A.; Pourshamsian, K.; Oliaey, A.; Hatamjafari, F. Theoretical investigations on the HOMO-LUMO gap and global reactivity descriptor studies, natural bond orbital, and nucleus-independent chemical shifts analyses of 3-phenylbenzo[d]-thiazole-2(3 H)-imine and its para -substituted derivatives: Solvent and substituent effects. *J. Chem. Res.* 2021, 45, 147.
- (43) Loveless, C. S.; Blanco, J. R.; Diehl, G. L.; Elbahrawi, R. T.; Carzaniga, T. S.; Braccini, S.; Lapi, S. E. Cyclotron Production and Separation of Scandium Radionuclides from Natural Titanium Metal and Titanium Dioxide Targets. J. Nucl. Med. 2021, 62 (1), 131.
- (44) Becke, A. D. A new mixing of Hartree-Fock and local density-functional theories. *J. Chem. Phys.* **1993**, 98 (2), 1372–1377.
- (45) Roy, L. E.; Hay, P. J.; Martin, R. L. Revised Basis Sets for the LANL Effective Core Potentials. *J. Chem. Theory Comput.* **2008**, 4 (7), 1029–1031.
- (46) Hehre, W. J.; Ditchfield, R.; Pople, J. A. Self—Consistent Molecular Orbital Methods. XII. Further Extensions of Gaussian—Type Basis Sets for Use in Molecular Orbital Studies of Organic Molecules. *J. Chem. Phys.* **1972**, *56* (5), 2257–2261.
- (47) Cossi, M.; Rega, N.; Scalmani, G.; Barone, V. Energies, structures, and electronic properties of molecules in solution with the C-PCM solvation model. *J. Comput. Chem.* **2003**, *24* (6), 669–681.
- (48) Frisch, M. J.; Trucks, G. W.; Schlegel, H. B.; Scuseria, G. E.; Robb, M. A.; Cheeseman, J. R.; Scalmani, G.; Barone, V.; Peterrson, G. A.; Nakatsuji, H.; Li, X.; Caricato, M.; Marenich, A.; Bloino, J.; Janesko, B. G.; Gomperts, R.; Mennucci, B.; Hratchian, H. P.; Ortiz, J. V.; Izmaylov, A. F.; Sonnenberg, J. L.; Williams-Young, D.; Ding, F.; Lipparini, F.; Egidi, F.; Goings, J.; Peng, B.; Petrone, A.; Henderson, T.; Ranasinghe, D.; Zakrzewski, V. G.; Gao, J.; Rega, N.; Zheng, G.; Liang, W.; Hada, M.; Ehara, M.; Toyota, K.; Fukuda, R.; Hasegawa, J.; Ishida, M.; Nakajima, T.; Honda, Y.; Kitao, O.; Nakai, T.; Vreven, T.; Throssell, K.; Montgomery, J. A., Jr.; Peralta, J. E.; Ogliaro, F.; Bearpark, M.; Heyd, J. J.; Brothers, E.; Kudin, K. N.; Staroverov, V. N.; Keith, T.; Kobayashi, R.; Normand, J.; Raghavarachi, K.; Rendell, A.; Burant, J. C.; Iyengar, S. S.; Tomasi, J.; Cossi, M.; Millam, J. M.; Klene, M.; Adamo, C.; Cammi, R.; Ochterski, J. W.; Martin, R. L.; Morokuma, K.; Farkas, O.; Foresman, J. B.; Fox, D. J. Gaussian 09; Gaussian Inc.: Wallingford, CT, 2016.
- (49) da Silva, E. F.; Svendsen, H. F.; Merz, K. M. Explicitly Representing the Solvation Shell in Continuum Solvent Calculations. *J. Phys. Chem. A* **2009**, *113* (22), 6404–6409.
- (50) Gupta, M.; da Silva, E. F.; Svendsen, H. F. Modeling Temperature Dependency of Amine Basicity Using PCM and SM8T Implicit Solvation Models. *J. Phys. Chem. B* **2012**, *116* (6), 1865–1875.